Radial lattice quantization of 3D ϕ^4 field theory

Richard C. Brower[‖]
Boston University, Boston, Massachusetts 02215, USA

George T. Fleming[†]
Yale University, Sloane Laboratory, New Haven, Connecticut 06520, USA

Andrew D. Gasbarro[‡]
AEC Institute for Theoretical Physics, Universität Bern, 3012 Bern, Switzerland

Dean Howarth[§]
Nuclear Science Division, Lawrence Livermore National Laboratory, Livermore, California 94550, USA

Timothy G. Raben[*]
Michigan State University, East Lansing, Michigan 48824, USA

Chung-I Tan[¶]
Brown University, Providence, Rhode Island 02912, USA

Evan S. Weinberg[**]
NVIDIA Corporation, Santa Clara, California 95050, USA

(Received 6 July 2021; accepted 27 September 2021; published 5 November 2021)

The quantum extension of classical finite elements, referred to as quantum finite elements (QFE) [R. C. Brower *et al.*, Lattice ϕ^4 field theory on Riemann manifolds: Numerical tests for the 2-d Ising CFT on $\mathbb{S}^2$, Phys. Rev. D **98**, 014502 (2018). and R. C. Brower *et al.*, Lattice dirac fermions on a simplicial Riemannian manifold, Phys. Rev. D **95**, 114510 (2017).], is applied to the radial quantization of 3D ϕ^4 theory on a simplicial lattice for the $\mathbb{R} \times \mathbb{S}^2$ manifold. Explicit counterterms to cancel the one- and two-loop ultraviolet defects are implemented to reach the quantum continuum theory. Using the Brower-Tamayo [Embedded Dynamics for ϕ^4 Theory, Phys. Rev. Lett. **62**, 1087 (1989).] cluster Monte Carlo algorithm, numerical results support the QFE ansatz that the critical conformal field theory (CFT) is reached in the continuum with the full isometries of $\mathbb{R} \times \mathbb{S}^2$ restored. The Ricci curvature term, while technically irrelevant in the quantum theory, is shown to dramatically improve the convergence, opening the way for high precision Monte Carlo simulation to determine the CFT data; operator dimensions, trilinear operator product expansion couplings, and the central charge.

DOI: 10.1103/PhysRevD.104.094502

I. INTRODUCTION

Numerous important aspects of nonperturbative quantum field theories are best understood on curved space-time manifolds. As an example, when a conformal field theory (CFT) on Euclidean $\mathbb{R}^d$ is mapped to the Riemann sphere, $\mathbb{S}^d$, the free energy gives direct access to the central charge [4]. Mapped alternatively to the cylinder [5], $\mathbb{R} \times \mathbb{S}^{d-1}$, "time" translations along the length of the cylinder are generated by the dilatation operator, giving direct access to conformal dimensions and the conformal partial-wave expansion [6]. Model building to search for potential new physics in composite Higgs or dark matter scenarios beyond the standard model increasingly focus on small

[*]Corresponding author.
rabentim@msu.edu
[†]geoerge.fleming@yale.edu
[‡]gasbarro@itp.unibe.ch
[§]howarth1@llnl.gov
[‖]brower@bu.edu
[¶]chung-i_tan@brown.edu
[**]eweinberg@nvidia.com

deformations from conformal infrared fixed points. These theories can be realized by lattice field theory [7–9] by adding Tev scale fermions, or described by Hamiltonian truncation [10] by adding mass deformations. Even for conventional Euclidean lattice QCD, the $\mathbb{R} \times \mathbb{S}^{d-1}$ manifold could be advantageous for describing scattering phase shifts with a spherical finite volume transverse to Euclidean time. A separate set of examples include nonperturbative studies of quantum gravity in the AdS/CFT framework [11], in which global Euclidean hyperbolic space maps at the boundary of AdS^{d+1} to a CFT on $\mathbb{S}^d$ or $\mathbb{R} \times \mathbb{S}^{d-1}$.

While there is a comprehensive literature, cf. [12–14], on the extension of Feynman's perturbation theory for renormalizable field theories to general smooth Riemann manifolds, the aforementioned problems stand to benefit greatly from a rigorous, nonperturbative method. One solution is the extension of lattice field theory methods beyond Euclidean flat space. Towards this solution, we have developed in previous works a quantum extension of classical finite elements by placing the lattice theory on a simplicial complex with appropriate counterterms, referred to as quantum finite elements (QFE) [1,2]. Within this framework, sophisticated algorithmic tools developed for lattice QCD can be leveraged for application to problems using curved manifolds.

In this work, we choose to study the classic prototype of 3D ϕ^4 in radial quantization on $\mathbb{R} \times \mathbb{S}^2$ in comparison with the well-studied 3D Ising CFT [15]. This serves as both an additional test of the QFE approach, as well as a demonstration of the utility of combining radial quantization and lattice methods. In this approach, translations, $t \to t + t_0$, along the cylinder correspond to exponential displacements in the radial distance $r = R\exp(t)$, allowing one to reach the equivalent of exponential scales on a finite lattice. We show that the exponentially decaying two-point correlators give direct access to eigenvalues of the dilatation operator, and Wilson coefficients of the conformal partial-wave expansion may be extracted from four-point correlators.

However, as pointed out by Cardy [16,17], for $d > 2$ a lattice implementation faces severe difficulties, because there is no uniform sequence of lattices approaching the spherical manifold, $\mathbb{S}^{d-1}$. A first attempt by Brower, Fleming, and Neuberger [18] placed the 3D Ising model on a cylindrical lattice $\mathbb{R} \times \mathcal{I}$ with the sphere $\mathbb{S}^2$ approximated by a uniformly triangulated icosahedron $\mathcal{I}$ as illustrated on the left side of Fig 1. While the results were encouraging, not surprisingly a small breaking of spherical symmetry was observed in the splitting of the $(2l+1)$-degenerate rotational multiplets. The third descendant $(l = 3)$ splits into two irreducible multiplets of the icosahedral group, even when extrapolated to the continuum limit. To remove this defect, a new lattice discretization method has been developed, referred to as QFE [2], conjectured to converge to the proper continuum limit for any renormalizable quantum field theory on a smooth Riemannian manifold.

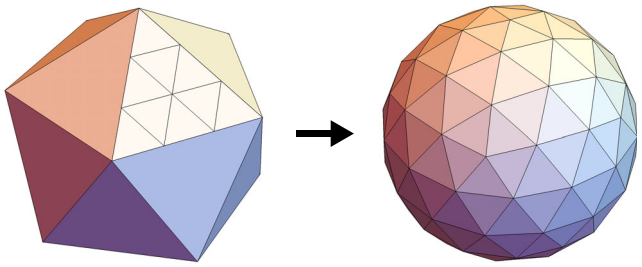

FIG. 1. The Lth level refinement of the icosahedron subdivides triangles into L^2 smaller triangles for a total of $N_\triangle = 20L^2$ faces, $E = 30L^2$ edges, and $N = 2 + 10L^2$ sites. Illustrated on the left is the $L = 3$ icosahedral refinement with $2 + 10L^2 = 92$ vertices and on the right subsequently projected onto the unit sphere.

To understand the nature of this conjecture it is useful to contrast our QFE simplicial lattice with the earlier pioneering results of Hasenbusch [19] carried out on the flat hypercubic lattice using almost identical Monte Carlo sampling. Hasenbusch demonstrates that the lattice ϕ^4 field theory has a critical line in the space of dimensionless bare couplings $m_0 = am, \lambda_0 = a\lambda$ with one relevant parameter and a Wilson Fisher fixed point at strong coupling as $a \to 0$. We conjecture that the QFE discretization—after renormalization by quantum counterterms up to two loops in perturbation theory, as we shall explain in detail below—contains the same critical surface in the bare coupling space. The numerical results presented in this work support this. As discussed in the conclusion, future simulation at higher precision as well as theoretical developments, e.g., for nonperturbative QFE counterterms, will seek to further strengthen the conjectured convergence.

The QFE construction begins by defining a series of refined simplicial lattices, which approach the target manifold, and a classical lattice action using the finite-element method (FEM) based on the discrete exterior calculus (DEC). While this is sufficient for classical solutions to the equation of motion, it fails in the quantum-path integral due to sensitivity to the irregular UV cutoff intrinsic to the simplicial approximation of the target manifold. To overcome this problem, explicit QFE counterterms are introduced in order to restore the exact nonperturbative quantum physics as the cutoff is removed.

To date this QFE method has been tested with numerical simulations for the 2D ϕ^4 theory on $\mathbb{S}^2$ and has been found to be in precise agreement with the exact solution of the minimal $c = 1/2$ Ising CFT [1]. The goals of this paper are to test the QFE method for ϕ^4 theory on $\mathbb{R} \times \mathbb{S}^2$ in comparison with the 3D Ising CFT and to demonstrate its potential to give high-precision lattice Monte Carlo predictions to extend and complement results from the conformal bootstrap [15,20].

II. CLASSICAL SIMPLICIAL LATTICE ACTION

Conformal field theories have an enlarged symmetry group, promoting the D-dimensional Euclidean-Poincaré group to the conformal group $O(d+1,1)$ or the isometries of the global AdS^{d+1} manifold. As a consequence, a CFT can equivalently be quantized after a Weyl transformation from a flat Euclidean manifold $\mathbb{R}^d$ to a cylinder $\mathbb{R}\times\mathbb{S}^{d-1}$,

$$ds^2_{\text{flat}} = dx^\mu dx^\mu = r^2[(d\log r)^2 + d\Omega^2_{d-1}] \xrightarrow{\text{Weyl}} ds^2_{\text{cylinder}} = dt^2 + R^2 d\Omega^2_{d-1}, \tag{1}$$

with a sphere of fixed radius R and flat coordinate $t=\log(r/R)$ along the length of the cylinder. In radial quantization the dilatation operator, which is conjugate to translations in radial time, t, plays the role of the Hamiltonian. The cylinder, illustrated in Fig. 7, resides on the boundary of AdS^{d+1} space. The problem, as in all lattice constructions, is to construct a discrete lattice action which is rigorously equivalent to the continuum-quantum path integral on the target manifold as the cutoff is removed. Since the radius of the sphere provides an intrinsic IR scale, the continuum limit for the conformal theory is now defined by the limit, $a/R\to 0$, relative to the UV cutoff at lattice spacing a.

We begin by implementing a finite element method discretization of the continuum action,

$$S_{\text{cont}} = \frac{1}{2}\int_{\mathcal{M}} d^dx\sqrt{g}[g^{\mu\nu}\partial_\mu\phi(x)\partial_\nu\phi(x) + \xi_0\mathbf{Ric}\phi^2(x) + m^2\phi^2(x) + \lambda\phi^4(x)], \tag{2}$$

for ϕ^4 theory on a curved Riemann manifold. The action includes a Ricci scalar term with nonzero coefficient, $\xi_0 = (d-2)/(4(d-1))$ for $d\geq 3$. For our radial quantization on $\mathbb{R}\times\mathbb{S}^{d-1}$, the Ricci term, $\mathbf{Ric} = (d-1)(d-2)/R^2$, is a constant determined by the radius of the sphere, and as such represents a shift in the mass. For the massless free theory ($m=\lambda=0$) in 3D, it is a relevant marginal operator required by conformality. As a result the free conformal scalar is gapped with a spectrum, $l(l+1)+1/4 = (l+1/2)^2$, that is the square of the spectrum, $l+1/2$, for a free massless Dirac operator. The dimension of the conformal scalar primary and its descendants is $\Delta_{\phi,l} = 1/2 + l$.

To construct the radial lattice action for $\mathbb{R}\times\mathbb{S}^2$, we introduce a sequence of simplicial lattice approximations to $\mathbb{S}^2$, as illustrated in Fig. 1. The simplicial lattice is refined by introducing finer triangulations on each icosahedral face and projecting onto geodesics on the sphere. This spherical lattice is copied uniformly along the $\mathbb{R}$ cylindrical axis with lattice spacing a_t. It is important to carefully introduce the FEM action in physical units relative to the radius, R, of the sphere,

$$S_{\text{FEM}} = \frac{a_t}{2}\left[\sum_{y\in\langle x,y\rangle}\frac{l^*_{xy}}{l_{xy}}(\phi_{t,x}-\phi_{t,y})^2 + \frac{\sqrt{g_x}}{4R^2}\phi^2_{t,x} + \sqrt{g_x}\left[\frac{(\phi_{t,x}-\phi_{t+1,x})^2}{a_t^2} + m^2\phi^2_{t,x} + \lambda\phi^4_{t,x}\right]\right], \tag{3}$$

with the Einstein summation convention for $x=1,2,\ldots,N$ for sites on each sphere and $t=1,2,\ldots,L_t$ along the length of the cylinder with periodic boundary conditions. On any 2D curved manifold this discrete scalar Laplacian on a triangular simplex coincides exactly with both linear FEM and with the form given earlier by Hamber and Williams [21–23] in the context of Regge calculus for dynamical gravity.

Another attractive approach is the use of DEC implementation on a simplicial complex and its Voronoi dual which again coincides with linear FEM and Regge calculus for $d=2$ but differs from linear elements for $d>2$. The use of DEC is implicit in the pioneering work by N. H. Christ, R. Friedberg, and T. D. Lee [24] in their work on random lattices in flat space. This formalism provides a natural extension for scalar fields in general dimensions as well as coupling to gauge [24] and Dirac fields [25]. In this context the l_{xy} are the lengths of the edges of triangles shown on the right side of Fig. 1, l^*_{xy} are the lengths of edges between circumcenters on the dual lattice, and $\sqrt{g_x}$ are the Voronoi dual areas at each site. On a general n-dimensional simplicial complex, the resultant DEC Laplace-Beltrami operator is

$$*\mathbf{d}*\mathbf{d}\phi_x = \frac{1}{|\sigma^*_0(x)|}\sum_{y\in\langle x,y\rangle}\frac{|\sigma^*_1(xy)|}{|\sigma_1(xy)|}(\phi_x-\phi_y), \tag{4}$$

with the replacement: $l_{xy}\to|\sigma_1(xy)|$, $l^*_{xy}\to|\sigma^*_1(xy)|$ and $\sqrt{g_x}\to|\sigma^*_0(x)|$. The discrete Hodge Star $(*)$ transfers differential forms between the simplicial lattice and Voronoi dual polytopes, weighted by appropriate volume elements. The reader is referred our earlier papers [1,2,26] and to the vast FEM literature for details [27].

It is important to appreciate the theoretical consequences of the discrete exterior calculus. When properly applied, DEC guarantees exact convergence of the simplicial action Eq. (3) to the classical action Eq. (2), and therefore all lattice solutions converge to solutions of the Euler-Lagrange partial differential equations as the cutoff is removed. Moreover, the DEC formalism extends naturally to higher dimensions with higher-spin gauge fields and Kähler-Dirac or staggered fermions. With the addition of a FEM spin connection, an extension to Wilson lattice fermions, including a domain wall with an extra flat direction, was formulated in Ref. [2].

In the next step, we follow the standard methods of numerical simulation by rewriting the lattice action in terms of dimensionless fields and parameters,

$$S = \frac{1}{2}\Bigg[\sum_{y\in\langle x,y\rangle}\frac{l^*_{xy}}{l_{xy}}(\phi_{t,x}-\phi_{t,y})^2 + \frac{a^2}{4R^2}\sqrt{g_x}\phi^2_{t,x} + \sqrt{g_x}\left[\frac{a^2}{a_t^2}(\phi_{t,x}-\phi_{t+1,x})^2 + m_0^2\phi^2_{t,x} + \lambda_0\phi^4_{t,x}\right]\Bigg]. \quad (5)$$

On a hypercubic lattice, with a uniform lattice spacing, a, this is equivalent to working in units so that $a = 1$. Here it is a bit subtler. The geometry of the manifold has introduced an explicit IR length scale through the radius of the sphere and two UV cutoffs; the longitudinal lattice spacing, a_t, and a characteristic edge length a^2 on the sphere. For convenience, we have defined a^2 relative to the average area of a Voronoi polytope, $A^* = \langle\sqrt{g_x}\rangle = a^2\sqrt{3}/2$, at each vertex. Of course, there are other possible choices such as average area of triangles, $A_\triangle \simeq A^*/2 = a^2\sqrt{3}/4$ or the average squared edge length, $\langle l^2_{xy}\rangle \simeq 0.752a^2$, which are equivalent to $\mathcal{O}(a^4/R^2)$.

To unambiguously recover the physical scales, we need to provide our change to dimensionless variables, $\tilde{g}_x$ and $\tilde{\phi}_{t,x}$,

$$\sqrt{g_x} = A^*\sqrt{\tilde{g}_x}, \qquad \phi_{t,x} = \tilde{\phi}_{t,x}/Z_0. \quad (6)$$

This fixes the mean lattice measure $\langle\sqrt{\tilde{g}_x}\rangle$ exactly to one and by choosing $Z_0^2 = a_t A^*/a^2$ preserves the form of the mass terms,

$$\frac{1}{N}\sum_x \sqrt{\tilde{g}_x} = 1, \qquad a_t\sqrt{g_x}m^2\phi^2_{tx} = \sqrt{\tilde{g}_x}a^2m^2\tilde{\phi}^2_{tx}. \quad (7)$$

Introducing a dimensionless mass ($m_0 = am$), coupling ($\lambda_0 = a^2\lambda/Z_0^2$), and dropping the tilde notation gives our lattice action in Eq. (5). In our simulation, we also set the bare speed of light to one; $c_0 = a/a_t = 1$. As a result, we have achieved the traditional advantage of setting all terms to $\mathcal{O}(1)$ in the lattice action, independent of the refinement.

Two consequences of our rescaling conventions should be noted. First, the rescaled weights of the kinetic term give

$$\sum_{\langle x,y\rangle} l^*_{xy}/l_{xy} = \frac{2}{3}(1+\epsilon_0)E, \quad (8)$$

when summed over E edges. The $2/3$ factor is a consequence of the equilateral triangulation of the icosahedron, each of which contributes exactly one to the sum. However, when the triangles are projected obliquely onto the sphere they are no longer equilateral so that the DEC weights increase the sum by a small geometrical fraction; $\epsilon_0 = 0.003285 + \mathcal{O}(a^2/R^2)$. We also note that using piecewise linear finite elements or the DEC, the $\mathcal{O}(a^2/R^2)$ corrections in the classical action (5) are not determined. At present in the quantum context, we see no compelling advantage to higher order elements.

Second, due to the intrinsic geometry of the manifold, the action still has explicit lattice spacing dependence in the coefficient of the lattice Ricci scalar. In our rescaling convention, Eq. (6), this coefficient is determined relative to area of the sphere,

$$a^2/R^2 = 4\pi a^2/(A^*N) = 8\pi/(\sqrt{3}N). \quad (9)$$

For the nonperturbative CFT in the continuum limit the Ricci term is an irrelevant operator due to the factor of a^2/R^2 combined with the known scaling dimension $\Delta_\epsilon > 1$ for ϕ^2. In our first extensive Monte Carlo simulations, we have dropped the Ricci term in Eq. (5) to demonstrate convergence to continuum CFT, as $a \to 0$. Although the Ricci term is not required, we demonstrate subsequently the major advantage of including it is to accelerate convergence to the continuum.

III. RESTORING SYMMETRIES IN THE QFT

Now we check whether or not our classical FEM action in Eq. (5), is capable of converging to the full quantum ϕ^4 theory on $\mathbb{R}\times\mathbb{S}^2$. To this end, we search for a critical surface in the bare coupling space (m_0^2, λ_0) with extensive Monte Carlo simulations. To search for the critical surface, we monitor the fourth-order Binder cumulant,

$$U_4(L, m_0^2, \lambda_0) = \frac{3}{2}\left[1 - \frac{\langle M^4\rangle}{3\langle M^2\rangle^2}\right], \quad (10)$$

of the magnetization $M = \sum_{t,x}\sqrt{g_x}\phi_{t,x}$, as we reduce the lattice spacing a. We impose periodic boundary conditions in t with fixed aspect ratio, $L_t/L = 4$. In the continuum limit, our Binder cumulant is normalized so that it approaches 0 in the extreme-disordered (Gaussian) phase and 1 in the extreme-ordered phase. A second-order critical surface is found where the Binder cumulant approaches a constant between 0 and 1 as the lattice spacing vanishes. We scan the relevant parameter m_0^2 at fixed $\lambda_0 = 0.2$.

As a base line, in the top panel in Fig. 2, we abandon the FEM weights by setting $l^*_{xy}/l_{xy} = 2/3$ and $\sqrt{g_x} = 1$. As in the radial 3D Ising simulation [18] with icosahedron triangulations on $\mathbb{R}\times\mathcal{I}$, there is apparently a well-defined critical theory. However as shown below in Fig. 3, the continuum fixed point exhibits only icosahedral irreducible multiplets, which break the full spherical symmetry at the level of the $l = 3$ descendant. The result is presumably a CFT on an the icosahedron cylinder, $\mathbb{R}\times\mathcal{I}$, not our intended target manifold, $\mathbb{R}\times\mathbb{S}^2$.

In the middle panel in Fig. 2, we restore the position dependent classical FEM weights in Eq. (5) for the simplicial lattice, but we now fail to locate a critical surface. For this study we have dropped the Ricci term and rescaled the fields to cancel ϵ_0 in Eq. (8). For values of $m_0^2 > -0.26906$, the cumulant trends towards $U_4 = 0$ for

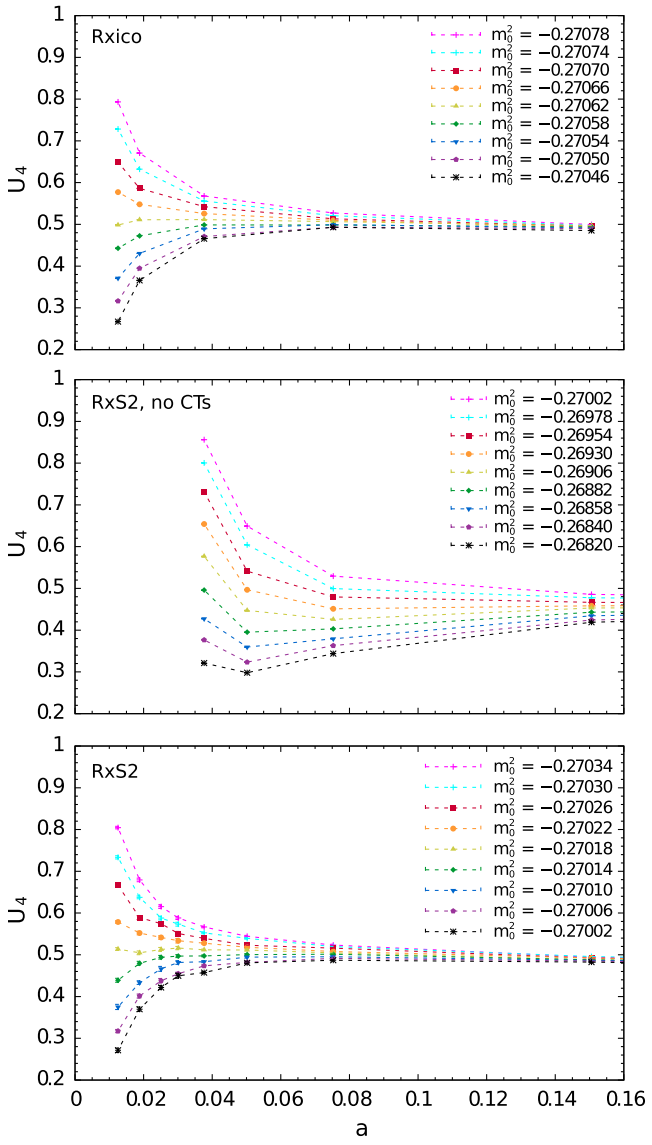

FIG. 2. Binder cumulant plotted against the lattice refinement for icosahedral spatial lattice (top) versus the spherical spatial lattice without (middle) and with counterterms (bottom). In all three cases, we searched in m_0^2 at fixed $\lambda_0 = 0.2$.

large a, but at smaller $a < 0.05$ the curves begin to turn around and will eventually oscillate. Ironically the FEM weights required for classical physics result in failure for quantum physics. Just as in our 2D application [1] on the Riemann sphere, $\mathbb{S}^2$, the problem is that the local FEM variations in the effective cutoff are amplified by the UV divergence of the quantum field theory. To overcome this problem, we add counterterms to our simplicial action, computed from spatially varying UV divergent lattice Feynman diagrams.

We need to define precisely how we convert the FEM action into the QFE action to compensate for quantum UV defects. Since ϕ^4 theory is super-renormalizable in three dimensions, there are a finite number of divergent

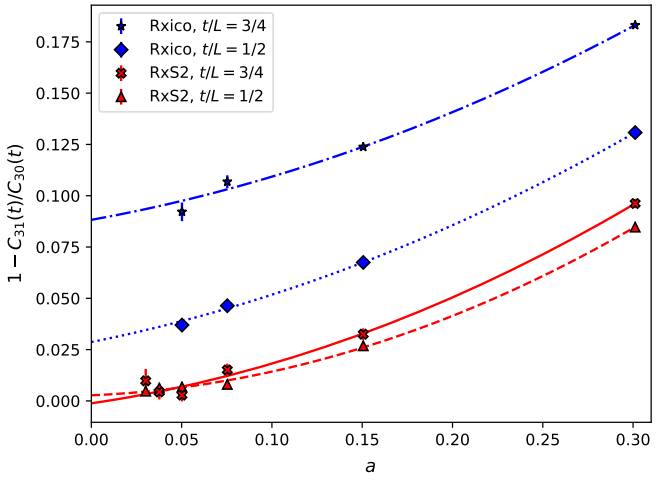

FIG. 3. Spherical symmetry breaking in the continuum limit for the icosahedral model on $\mathbb{R} \times \mathcal{I}$ (**Rxico**) compared with QFE on $\mathbb{R} \times \mathbb{S}^2$ (**RxS2**) for the $l = 3$ correlator at separations $t/L = 1/2, 3/4$.

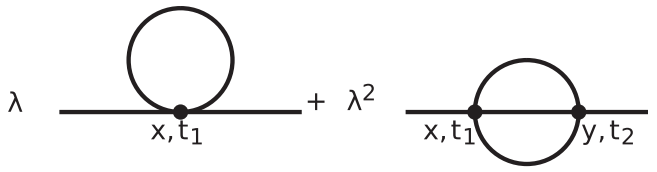

FIG. 4. The one- and two-loop UV divergent diagrams contributing to the mass renormalization in 3D.

diagrams, illustrated in Fig. 4: a one-loop linear divergence and a two-loop logarithmic divergence.

To construct the simplicial Feynman diagrams in Fig. 4, we compute numerically the lattice propagator, $G_{t_1,x;t_2,y}$, for the free theory at $m_0 = 0$ including the Ricci term, which is required by conformal symmetry and to act as IR regulator on the sphere. The result to second order is an effective action,

$$\Gamma_{\text{eff}} = \Gamma_0 + 6\lambda_0\sqrt{g_x}G_{t,x;t,x}\phi_{t,x}^2 - 24\lambda_0^2\sqrt{g_x}\phi_{t_1,x}G_{t_1,x;t_2,y}^3\phi_{t_2,y}\sqrt{g_y}. \quad (11)$$

The counterterms will be designed to exactly cancel the rotational breaking in the relevant operators in our lattice action.

Not only is the one-loop lattice diagram local, it is also finite in lattice units. This finiteness for power divergences is a general feature of lattice perturbation theory. We subtract the rotational symmetric piece to isolate the breaking term,

$$\delta G_x \equiv G_{t,x;t,x} - \frac{1}{N}\sum_{x=1}^{N}\sqrt{g_x}\,G_{t,x;t,x}, \quad (12)$$

which is independent of t by translation invariance along the cylinder. The two-loop term in Fig. 4 gives a nonlocal product $\phi_{t_1,x}\phi_{t_2,y}$. However, after subtracting the rotational-symmetric piece, we find that the nonlocal behavior is exponentially damped in units of the lattice spacing—or in the jargon of lattice field theory, the correction is local but not ultralocal. So to leading order in a, the dominant contribution is local and can be isolated by defining

$$\delta G_x^{(3)} \equiv \sum_{t',y} \sqrt{g_y}\left[G^3_{t,x;t',y} - \frac{1}{N}\sum_{x=1}^{N}\sqrt{g_x}\, G^3_{t,x;t',y}\right]. \quad (13)$$

The sum over t', y cancels a rotational symmetric logarithmic divergence, yielding a finite position dependent counterterm as in the case of the one-loop counterterm introduced for 2D ϕ^4 theory on $\mathbb{S}^2$. The reader is referred to Ref. [1] for details.

As a result, we propose a new QFE action

$$S_{\rm QFE} = S - \sum_{t,x}\sqrt{g_x}[6\lambda_0\delta G_x - 24\lambda_0^2\delta G_x^{(3)}]\phi^2_{t,x}, \quad (14)$$

relative to the classical FEM lattice action, S, in Eq. (5). By tuning to the weak-coupling fixed point, this QFE action should match the full renormalized perturbation following the Wilsonian-renormalization procedure in the same fashion as on a regular hypercubic lattice. Moreover we see the new QFE lattice action in the bottom panel of Fig. 2 does appear to have a well-defined critical surface. Dropping the Ricci term in Eq. (8), the Binder cumulant is studied up to lattice sizes of $L = 96$. We intersect the critical surface at $\lambda_0 = 0.2$ and $m_0^2 \simeq -0.27018(4)$, which we now fix as a good approximation to the continuum critical couplings at zero lattice spacing.

We now conjecture that our QFE lattice action Eq. (14), tuned to the critical surface, also converges to the exact nonperturbative CFT as the cutoff is removed. In the absence of a proof we support this QFE conjecture with numerical simulations. While this is the standard Wilson-renormalization procedure used extensively on the hypercubic lattice in flat space, we acknowledge that this a nontrivial extension for our QFE action on curved manifolds, which warrants further theoretical and higher-precision numerical investigation.

Next, we check the restoration of SO(3) spatial rotational symmetry by examining the two-point correlator in the $\mathbb{Z}^2$-odd channel on the critical surface,

$$C_{l,m_1,m_2}(t_1 - t_2) = \langle \phi_{t_1,lm_1}\phi_{t_2,lm_2}\rangle, \quad (15)$$

projected onto partial waves on the sphere, $\phi_{t,lm} = \sum_x \sqrt{g_x}\phi_{t,x}Y_{lm}[x]$. The spherical harmonics are defined by evaluating the continuum functions at the discrete sites x. In the continuum limit, spherical symmetry implies $C_{l,m_1,m_2}(t) = \delta_{m_1,m_2}c_l(t)$, with $(2l+1)$ degeneracy for SO(3) irreducible representations. The first three SO(3) representations, $l = 0$, 1, 2, are also irreducible in the icosahedral group. At the $l = 3$ level, the seven-dimensional SO(3) representation splits at finite lattice spacing into a direct sum of a three ($3T$) and a four ($3G$)-dimensional irreducible representation in the icosahedral group. We examine the diagonal elements $m_1 = m_2 = 0$ and $m_1 = m_2 = 1$ denoted by $C_{30}(t)$ and $C_{31}(t)$, which are components entirely in the $3T$- and $3G$-icosahedral representations respectively.

In Fig. 3, we plot the normalized error in rotational symmetry, $1 - C_{31}(t)/C_{30}(t)$, at two fixed physical time slices $t/L = 1/2$ and $t/L = 3/4$ as a function of the lattice spacing a. A quadratic function is fit to each case to extrapolate to the continuum limit. Comparing the critical theory on $\mathbb{R}\times\mathcal{I}$ and on $\mathbb{R}\times\mathbb{S}^2$, we see that without FEM weights and counterterms, the icosahedral breaking persists to the continuum limit as expected, whereas for our QFE action in Eq. (14), including the one- and two-loop counterterms, the SO(3) symmetry is recovered.

IV. RICCI IMPROVED TWO-POINT CORRELATOR

Conformal symmetry completely determines the form of the two-point function of primary operators, which for a scalar in radial quantization is given by

$$\langle\phi(t_1,r_1)\phi(t_2,r_2)\rangle = \frac{1}{(2\cosh t_{12} - 2\cos\theta_{12})^{\Delta_\phi}}, \quad (16)$$

with $t_{12} = |t_1 - t_2|$ and $\cos\theta_{12} = r_1\cdot r_2$ the relative coordinates on the cylinder in Fig 7. Up to an overall normalization convention, the correlator is fixed by the

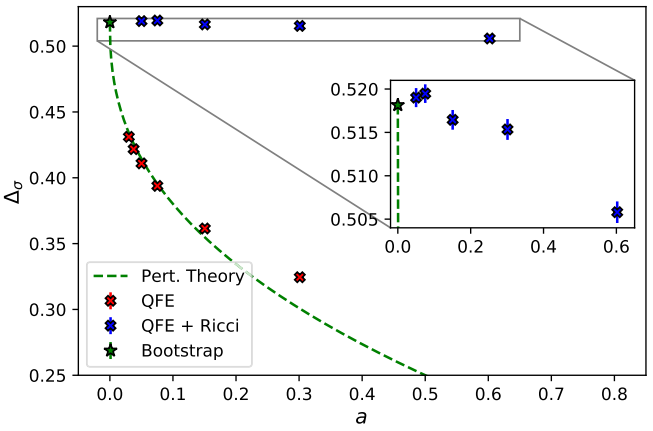

FIG. 5. Scaling dimension of lowest Z_2 odd scalar primary σ as a function of the lattice spacing, computed with (blue crosses) and without (red crosses) the Ricci term in the QFE action. Fixing the $\Delta_\sigma = 0.5181$ at $a = 0$ (green star) including Ricci term in perturbation (green dashes) fits well the lattice-spacing dependence.

scaling dimension Δ_ϕ of the primary operator. Having tested the restoration of spherical symmetry approaching the critical surface at $m_0^2 \simeq -0.27018(4)$ and $\lambda_0 = 0.2$, this correlator provides a stringent test of conformal symmetry for the continuum limit of the QFE lattice.

The lowest primary in the Z_2-odd sector couples to the lattice field $\phi_{t,x}$ and must scale with the conformal dimension Δ_σ with unit spacing of its descendants $\Delta_{\sigma,l} = \Delta_\sigma + l$ for $l = 1, 2, 3, \ldots$ in the continuum limit. The lattice correlator is projected onto partial waves on the sphere as in Eq. (15) and fit to exponentials, $\exp[-\mu_l t_{12}]$, for large $t_{12} = |t_1 - t_2|$. The lattice masses, μ_l, are related to the scaling dimension by $\mu_l = a_t \Delta_{\sigma,l} = c_R a \Delta_{\sigma,l}$ in terms of a renormalized speed of light c_R relative to the bare value c_0 which we set to 1 in the classical limit. We may fix the renormalized c_R either by enforcing the integer spacing of descendants in the continuum limit or by matching the conserved dimension $\Delta_T = 3$ for the energy-momentum tensor in the OPE expansion of the four-point function in Eq. (25).

The results for $\Delta_{\sigma,l}$ as function of a are given in Fig. 6. All the data is in a limited range of lattice spacing $a \in [0.03, 0.15]$ corresponding to lattice sizes of $L \in [8, 40]$ on the periodic cylinder with aspect ratio $L_t/L = 16$. By computing the correlation function on $\mathcal{O}(10^8)$ statistically independent configurations with an improved cluster estimator [3], we achieve statistical errors for the scaling

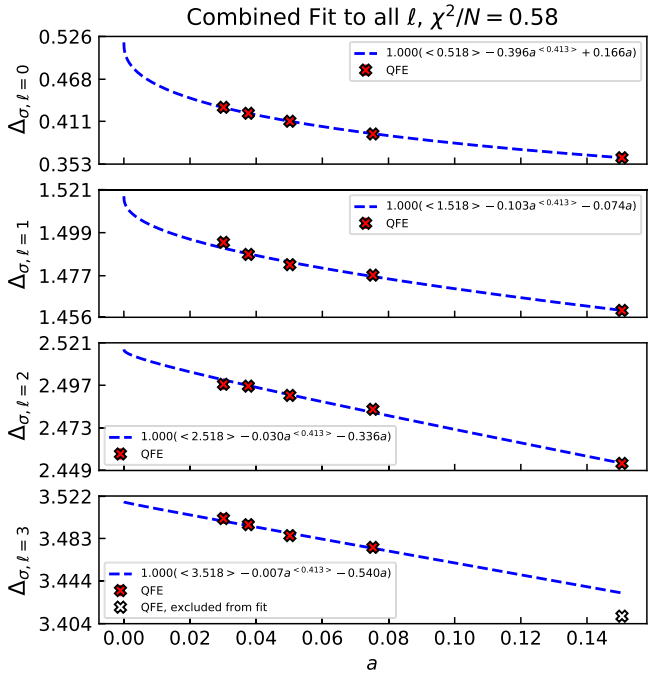

FIG. 6. Lowest Z_2 odd-scaling dimension, $\Delta_{\sigma,l}$, as a function of lattice spacing, a, for the lowest four angular-momentum values. Quantities in angle brackets are held fixed in the continuum limit fits. Where not visible, statistical error bars are smaller than markers.

dimension on the order of 0.1%. With such high statistics, our initial fits (not shown) clearly identified a lattice artifact term scaling as $\mathcal{O}(a^{0.40})$ giving rise to an infinite slope as one approaches the continuum limit. This is consistent at the 1% level with the scaling dimension of the composite operator, $:\phi_{x,t}^2:$ ($\Delta_\epsilon = 1.4126$), implying a cut off dependence, $\mathcal{O}(a^{\Delta_\epsilon - 1}) = \mathcal{O}(a^{0.4126})$, when the Ricci term is not included in the lattice action. Indeed to check this idea, we parametrize the fits shown in Fig. 6 to

$$\Delta_{\sigma,l}(a) = c(\Delta_\sigma + l + A_l a^{\Delta_\epsilon - 1} + B_l a), \tag{17}$$

determining the constants c, A_l, and B_l by a simultaneous fit to $l = 0$, 1, 2, 3 while setting the dimensions to their continuum values; $\Delta_\sigma \simeq 0.5181$ and $\Delta_\epsilon \simeq 1.4126$. The linear term was added to model subleading lattice artifacts beyond the irrelevant Ricci scaling. For the coarsest lattice spacing at the $l = 3$ level, we see that there may be sensitivity to yet further lattice artifacts, so we omit this point from the fit.

The result of the fit is shown by the blue dashed curves in Fig. 6, with the best-fit values of the coefficients reported in the legend. We remark that the best-fit value for the renormalized speed of light is very close to 1. The small $\chi^2/N = 0.58$ indicates that the Ricci term accurately captures the leading lattice artifact behavior, playing an important role in the continuum extrapolation despite being irrelevant. The correlator clearly converges to the conformal multiplet—albeit slowly with the Ricci term excluded from the simulation—as indicated by an accurate recovery of the descendent relation up to $l = 3$ and consistency with the bootstrap value for Δ_σ [28].

To check quantitatively the role of the Ricci term in approaching the continuum discovered in Fig. 6, we carry out two additional studies. First, we treat the Ricci term, $\delta S = -(a^2/(8R^2))\sqrt{g_x}\phi_{t,x}^2$, as a small perturbation near the continuum limit. To first order this shifts the scaling dimensions by

$$\delta\Delta_{\sigma,l} = -\frac{a^2}{8R^2}\langle \Delta_{\sigma,l}|\sqrt{g_x}\phi_{t,x}^2|\Delta_{\sigma,l}\rangle_c, \tag{18}$$

where the sum over x is implied. The right-hand side is independent of t by translation invariance down the cylinder. The form factor on the right-hand side remains a nonperturbative function of λ_0. We have computed the matrix element in our Monte Carlo simulation for $l = 0$ and $l = 1$ through a standard ratio method,

$$\langle \Delta_{\sigma,l}|\sqrt{g_x}\phi_{t,x}^2|\Delta_{\sigma,l}\rangle_c \simeq \frac{\langle \phi_{t_1,lm}\sqrt{g_x}\phi_{t,x}^2\phi_{t_2,lm}\rangle_c}{\langle \phi_{t_1,lm}\phi_{t_2,lm}\rangle} \tag{19}$$

for the connected piece, as $t_1/t_2 \to +/-\infty$, which implements for the CFT the standard operator-state correspondence map. The resultant,

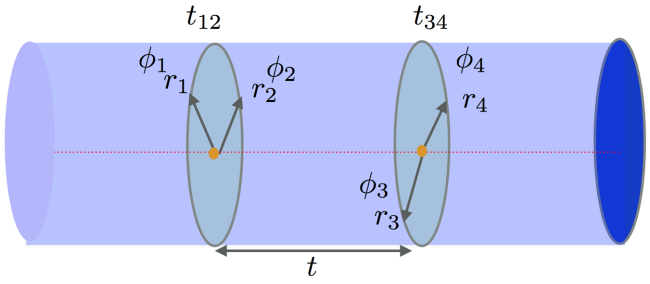

FIG. 7. The operator product expansion (OPE) for the four-point function on the cylinder is computed by placing the field on two spheres separated by $t = |t_{12} - t_{13}|$.

$$\delta\Delta_{\sigma,l=0} = -0.3777(38)a^{\Delta_\epsilon - 1}, \tag{20}$$

$$\delta\Delta_{\sigma,l=1} = -0.083(10)a^{\Delta_\epsilon - 1}, \tag{21}$$

are in reasonable agreement with the coefficients found by fitting Eq. (17) given in Fig. 6. The perturbative prediction in Eq. (20), shown in Fig. 5 by the green dashed curve, has zero free parameters after fixing to the continuum value $\Delta_\sigma = 0.5181$ at $a = 0$. The Ricci term describes the a dependence of the data of the original simulation accurately at small $a < 0.2$.

Next we carried out a modest first simulation including the Ricci term in an improved QFE action for lattice spacings $a \in [0.05, 0.6]$ on $\mathcal{O}(10^7)$ statistically independent configurations. The blue markers in Fig. 5 show the results from the simulation using the Ricci improved action compared to the red markers showing the original high statistics simulation omitting the Ricci term. The improved action simulation, highlighted in the insert, shows a dramatic improvement at lattice spacings $a < 0.2$, reducing finite lattice cutoff effects by two orders of magnitude and achieving an accuracy for the scaling dimension $\Delta_\sigma = 0.518(2)$ at about 0.5% and in agreement with the bootstrap value. In passing we note that for 2D ϕ^4 on $\mathbb{S}^2$ [1], this correction was not required, as expected since the coefficient of the Ricci term for d = 2 vanishes.

V. OPERATOR PRODUCT EXPANSION

The full content of a CFT requires computing data for both the dimension of operators and the three-point coupling that appears first in the four-point function OPE. Here we summarize our method to extract the same parameters from QFE simulations on $\mathbb{R} \times \mathbb{S}^2$. Radial quantization is well suited to study the OPE.

The invariant amplitude for identical scalars, $\phi_1 + \phi_2 \to \phi_3 + \phi_4$, is

$$g(u, v) = \frac{\langle \phi_{t_1,r_1} \phi_{t_2,r_2} \phi_{t_3,r_3} \phi_{t_4,r_4} \rangle}{\langle \phi_{t_1,r_1} \phi_{t_2,r_2} \rangle \langle \phi_{t_3,r_3} \phi_{t_4,r_4} \rangle}, \tag{22}$$

in terms of the standard cross ratios, u and v. In radial quantization it is more convenient to choose τ, α coordinates,

$$\cosh(\tau) = \frac{1 + \sqrt{v}}{\sqrt{u}}, \qquad \cos(\alpha) = \frac{1 - \sqrt{v}}{\sqrt{u}}, \tag{23}$$

where for large τ and fixed angle, $\sqrt{u} \simeq 4\exp(-\tau)$. To extract OPE terms, we place two incoming fields on one sphere and two outgoing on a second separated by $t = t_{12} - t_{34}$ as illustrated in Fig 7. Propagation is given by the dilatation operator D, so that the invariant amplitude is

$$g(\tau, \alpha) = \langle |r_1 - r_2|^{2\Delta_\sigma} \phi_1 \phi_2 e^{-tD} |r_3 - r_4|^{2\Delta_\sigma} \phi_3 \phi_4 \rangle,$$

where the continuum two-point functions have been inserted using the normalization convention in Eq. (16). It should be noted that the time (t) separation along the cylinder is not in general a conformal invariant as it is conjugate to the dilatation operator.

However, by choosing a special frame with antipodal points [29] on each unit sphere, the time separation t and angle θ are now mapped to invariants,

$$\cosh(\tau) = \cosh(t), \qquad \cos(\alpha) = \hat{r}_1 \cdot \hat{r}_3 = \cos(\theta), \tag{24}$$

and the OPE expansion for $d = 3$ is given as the partial waves expansion,

$$g(\tau, \alpha) = 1 + \sum_{\Delta_l, l=0,2,\cdots} \lambda^2_{\Delta_l} e^{-\Delta_l t} P_l(\cos\theta), \tag{25}$$

where the leading contribution from the identity operator is normalized to be unity. Expanding conformal blocks into partial waves [30], the couplings and dimensions of the descendants are fixed by their primaries and therefore restricting our fitting parameters to CFT data. (For $d \neq 3$, one replaces $P_l(\cos\theta)$ by Gegenbauer polynomials, $C^\nu_l(\cos\theta)$, with $\nu = d/2 - 1$.)

We are particularly interested in the contribution from the stress-energy tensor, with $l = 2$ and $\Delta_T = d$ to determine the central charge C_T. Following Dolan and Osborn [31], the coupling to the energy momentum tensor in Eq. (25) is

$$\lambda^2_{\Delta_T} = \frac{4^{\Delta_T} \Delta^2_\sigma \Delta^2_T}{C_T d(d-1)} = \frac{96\Delta^2_\sigma}{C_T}. \tag{26}$$

Note in 2D the common practice is to use $c = C_T/2$ so the free field is $c = 1$. We note in passing that the bootstrap's c-minimization hypothesis for the central charge gives only a few percent reduction, $C_T/C_T^{\text{free}} = 0.946534(11)$, relative to the free theory $C_T^{\text{free}} = d/(d-1) = 3/2$. Indeed all the dimensions of the lowest primaries in the 3D Isings CFT and their couplings, with the exception of Δ_ϵ, are within a

few percent of the free (or generalized mean field) value, so significant comparisons to the bootstrap require high precision.

To achieve this in our future high precision simulations, the Ricci QFE action will be used along with additional improvement schemes common to numerical lattice field theory. Since no lattice operator is a pure primary, we will construct improved lattice sources to better approximate primary operators. As a typical example, in the lowest odd Z_2 scalar sector, with almost no additional cost an improved estimator in the cluster algorithm can measure a 2×2 matrix of correlator: $C_{ij} = \langle \mathcal{O}_i(t_1 x_1) \mathcal{O}_j(t_1, x_2) \rangle$ for $\mathcal{O}_i(t, x) = \{\phi(t, x), \phi^3(t, x)\}$. In principle, as the lattice spacing $a \to 0$, the mixing is $\mathcal{O}((a/R)^{\Delta_{\sigma'} - \Delta_\sigma})$. By diagonalizing the 2×2 matrix, the lowest state is an improved variational operator for σ primary at finite lattice spacing. Using this operator will further reduce the lattice-spacing errors in the four-point function.

VI. FUTURE DIRECTIONS

Based on the numerical evidence in this letter, we believe our QFE lattice theory does converge to the continuum CFT as the cutoff is removed. The current simulation due to the efficiency of the cluster algorithm generated $\mathcal{O}(10^8)$ uncorrelated configurations that allowed us to identify the importance of including the Ricci term in the action. Next we plan to proceed to much higher precision numerical investigations to support the QFE lattice method against the best CFT data from the conformal bootstrap [15].

In particular we seek both stronger numerical and theoretical support for our quantum counterterms. We find it surprising that even in a super-renormalizable theory, we appear to restore the spherical manifold with the counterterms extracted from perturbation theory. One possibility is that these counterterms are only truly valid if we take the continuum limit at fixed renormalized mass and coupling m, λ, by scaling the bare dimensionless lattice parameters, $m_0 = am, \lambda_0 = a\lambda$, to zero. This is a viable alternative method to implement our QFE algorithm. Indeed by simulating at fixed m_0, λ_0 and taking $a \to 0$ as in this work, we may eventually reach a sufficiently small lattice spacing at which the counterterms fail. At current precision and lattice volumes this has not been observed, but it remains a viable interpretation. Also we are seeking a nonperturbative definition of counterterms, e.g., with Wilson flow [32], capable of extending the critical surface to span the full range of bare couplings, as observed by Hasenbusch [19] on a regular cubic lattice. Support for this requires new theoretical developments, backed up by higher precision numerical data.

Stringent comparison between QFE and the conformal bootstrap is interesting in its own right. Either agreement or disagreement could have fundamental consequences, since the two are based on radically different methods and assumptions. The QFE approach identifies a specific target quantum field theory as the cutoff is removed, whereas the bootstrap tightly constraints a generic class of theories by combining exact inequalities on a truncated operator expansion with the observation that simple known theories nearly saturate the constraints, supplemented for example by the c-Minimization procedure [15]. Agreement between the two approaches would go a long way to supporting the validity of both. Disagreement will begin a fundamental search for a better theoretical understanding to hopefully remove the discrepancies.

By including fermions and gauge fields on the simplicial complex, we believe QFE lattice theory should apply to any quantum field theory that posses a renormalizable perturbative expansion on a smooth Euclidean-Riemann manifold [14]. Conformal and special integrable models provide stringent tests for QFE, but the general approach is equally applicable to theories with massive deformations. The mass deformation naturally induces a spectral flow from eigenvalues of the Dilation operator to the Hamiltonian, e.g., operator dimensions (Δ) to masses (m) respectively in the continuum limit; $1/R \ll m \ll 1/a$. QFE is complimentary to the expanding repertoire of Hamiltonian truncation [10] and the conformal truncation [33] methods that also seek a nonperturbative computation moving adiabatically away from CFT fixed points.

Particularly interesting in this regard is the application of QFE to 4D non-Abelian gauge theories, which are under consideration as models for composite Higgs or dark matter [34], with enough fermionic flavors to be in or near the IR conformal window at strong coupling. Supersymmetric conformal examples are also under consideration. QFE methods should have an even wider range of applications to quantum gravity, for example in anti–de Sitter space [35] or the Regge formulation of simplicial gravity interacting with matter. None of these extensions are easy or guaranteed to work, but we believe that the current success with 3D ϕ^4 theory suggests a way forward to test more complicated field theories.

ACKNOWLEDGMENTS

We thank Casey Berger, Cameron Cogburn, Joel Giedt, Simeon Hellerman, Ami Katz, Kantaro Ohmori, and Domenico Orlando for useful discussions. This work was supported by the U.S. Department of Energy (DOE) under Award No. DE-SC0015845 for R. C. B. and under Award No. DE-SC0019061 for G. T. F. T. G. R. acknowledges support from the Office of the Senior Vice President for Research and Innovation at Michigan State University. A. D. G. acknowledges support from SNSF Grant No. 200021_175761.

[1] R. C. Brower, M. Cheng, E. S. Weinberg, G. T. Fleming, A. D. Gasbarro, T. G. Raben, and C.-I. Tan, Lattice ϕ^4 field theory on Riemann manifolds: Numerical tests for the 2-d Ising CFT on $\mathbb{S}^2$, Phys. Rev. D **98**, 014502 (2018).

[2] R. C. Brower, E. S. Weinberg, G. T. Fleming, A. D. Gasbarro, T. G. Raben, and C.-I. Tan, Lattice dirac fermions on a simplicial Riemannian manifold, Phys. Rev. D **95**, 114510 (2017).

[3] R. Brower and P. Tamayo, Embedded Dynamics for ϕ^4 Theory, Phys. Rev. Lett. **62**, 1087 (1989).

[4] S. S. Gubser and I. R. Klebanov, A Universal result on central charges in the presence of double trace deformations, Nucl. Phys. **B656**, 23 (2003).

[5] S. Rychkov, EPFL Lectures on Conformal Field Theory in $D \geq 3$ Dimensions, SpringerBriefs in Physics (Springer International Publishing, New York City, 2016).

[6] F. A. Dolan and H. Osborn, Conformal partial waves and the operator product expansion, Nucl. Phys. **B678**, 491 (2004).

[7] R. C. Brower, A. Hasenfratz, C. Rebbi, E. Weinberg, and O. Witzel, Composite Higgs model at a conformal fixed point, Phys. Rev. D **93**, 075028 (2016).

[8] Z. Fodor, K. Holland, J. Kuti, D. Nogradi, and C. Schroeder, Nearly conformal gauge theories in finite volume, Phys. Lett. B **681**, 353 (2009).

[9] T. Appelquist *et al.*, Stealth dark matter: Dark scalar baryons through the Higgs portal, Phys. Rev. D **92**, 075030 (2015).

[10] S. Rychkov and L. G. Vitale, Hamiltonian truncation study of the ϕ^4 theory in two dimensions, Phys. Rev. D **91**, 085011 (2015).

[11] J. M. Maldacena, The large N limit of superconformal field theories and supergravity, Int. J. Theor. Phys. **38**, 1113 (1999); Adv. Theor. Math. Phys. **2**, 231 (1998).

[12] I. Jack and H. Osborn, Background field calculations in curved space-time. 1. General formalism and application to scalar fields, Nucl. Phys. **B234**, 331 (1984).

[13] I. Jack, Background field calculations in curved space-time. II. Application to a pure gauge theory, Nucl. Phys. **B234**, 365 (1984).

[14] M. Luscher, Dimensional regularization in the presence of large background fields, Ann. Phys. (N.Y.) **142**, 359 (1982).

[15] S. El-Showk, M. F. Paulos, D. Poland, S. Rychkov, D. Simmons-Duffin, and A. Vichi, Solving the 3d Ising model with the conformal bootstrap II. c-Minimization and precise critical exponents, J. Stat. Phys. **157**, 869 (2014).

[16] J. L. Cardy, Conformal invariance and universality in finite-size scaling, J. Phys. A **17**, L385 (1984).

[17] J. L. Cardy, Universal amplitudes in finite-size scaling: Generalisation to arbitrary dimensionality, J. Phys. A **18**, L757 (1985).

[18] R. C. Brower, G. T. Fleming, and H. Neuberger, Lattice radial quantization: 3D Ising, Phys. Lett. B **721**, 299 (2013).

[19] M. Hasenbusch, A Monte Carlo study of leading order scaling corrections of ϕ^4 theory on a three-dimensional lattice, J. Phys. A **32**, 4851 (1999).

[20] S. El-Showk, M. F. Paulos, D. Poland, S. Rychkov, D. Simmons-Duffin, and A. Vichi, Solving the 3d ising model with the conformal bootstrap, Phys. Rev. D **86**, 025022 (2012).

[21] H. W. Hamber and R. M. Williams, Simplicial gravity coupled to scalar matter, Nucl. Phys. **B415**, 463 (1994).

[22] H. W. Hamber and R. M. Williams, Simplicial quantum gravity with higher derivative terms: Formalism and numerical results in four-dimensions, Nucl. Phys. **B269**, 712 (1986).

[23] H. W. Hamber and R. M. Williams, Two-dimensional simplicial quantum gravity, Nucl. Phys. **B267**, 482 (1986).

[24] N. Christ, R. Friedberg, and T. Lee, Random lattice field theory: General formulation, Nucl. Phys. **B202**, 89 (1982).

[25] R. Friedberg, T. D. Lee, and H.-c. Ren, Fermion field on a random lattice, Prog. Theor. Phys. Suppl. **86**, 322 (1986).

[26] A. D. Gasbarro, Studies of conformal behavior in strongly interacting quantum field theories, Other thesis, Yale University, 2019.

[27] D. N. Arnold, R. S. Falk, and R. Winther, Finite element exterior calculus: From hodge theory to numerical stability, Bull. Am. Math. Soc. **47**, 281 (2010).

[28] F. Kos, D. Poland, and D. Simmons-Duffin, Bootstrapping mixed correlators in the 3D Ising model, J. High Energy Phys. 11 (2014) 109.

[29] M. Hogervorst and S. Rychkov, Radial coordinates for conformal blocks, Phys. Rev. D **87**, 106004 (2013).

[30] M. Hogervorst, Dimensional reduction for conformal blocks, J. High Energy Phys. 09 (2016) 017.

[31] F. A. Dolan and H. Osborn, Conformal four point functions and the operator product expansion, Nucl. Phys. **B599**, 459 (2001).

[32] M. Lscher, Properties and uses of the Wilson flow in lattice QCD, J. High Energy Phys. 08 (2010) 071; Erratum, 03 (2014) 092.

[33] N. Anand, A. L. Fitzpatrick, E. Katz, Z. U. Khandker, M. T. Walters, and Y. Xin, Introduction to lightcone conformal truncation: QFT dynamics from CFT data, arXiv:2005.13544.

[34] R. C. Brower, A. Hasenfratz, E. T. Neil, S. Catterall, G. Fleming, J. Giedt, E. Rinaldi, D. Schaich, E. Weinberg, and O. Witzel, Lattice gauge theory for physics beyond the standard model, Eur. Phys. J. A **55**, 198 (2019).

[35] R. C. Brower, C. V. Cogburn, A. L. Fitzpatrick, D. Howarth, and C.-I. Tan, Lattice setup for quantum field theory in AdS_2, arXiv:1912.07606.